Electrostatically "Patchy" Coatings via Cooperative Adsorption of Charged Nanoparticles

ARTICLE *in* JOURNAL OF THE AMERICAN CHEMICAL SOCIETY · JANUARY 2008

Impact Factor: 12.11 · DOI: 10.1021/ja075456w · Source: PubMed

5 AUTHORS, INCLUDING:

Stoyan K. Smoukov
University of Cambridge
64 PUBLICATIONS **1,571** CITATIONS
SEE PROFILE

Kyle J M Bishop
Pennsylvania State University
80 PUBLICATIONS **2,974** CITATIONS
SEE PROFILE

Alexander M. Kalsin
Russian Academy of Sciences
25 PUBLICATIONS **1,093** CITATIONS
SEE PROFILE

J|A|C|S
ARTICLES
Published on Web 11/28/2007

Electrostatically "Patchy" Coatings via Cooperative Adsorption of Charged Nanoparticles

Stoyan K. Smoukov, Kyle J. M. Bishop, Bartlomiej Kowalczyk, Alexander M. Kalsin, and Bartosz A. Grzybowski*

Contribution from the Departments of Chemistry and Chemical and Biological Engineering, Northwestern University, 2145 Sheridan Road, Evanston, Illinois 60208

Received July 21, 2007; E-mail: grzybor@northwestern.edu

Abstract: Solutions containing oppositely charged nanoparticles (NPs) deposit "patchy" coatings of alternating charge distribution on various types of materials, including polymers, elastomers, and semiconductors. Surface adsorption of the NPs is driven by cooperative electrostatic interactions and does not require chemical ligation or layer-by-layer schemes. The composition and the quality of the coatings can be regulated by the types, the charges, and the relative concentrations of the NPs used and by the pH. Dense coatings form on flat, curvilinear, or micropatterned surfaces, are stable against common chemicals for prolonged periods of time, and can be used in applications ranging from bacterial protection to plasmonics.

Introduction

Coatings composed of or containing various types of nanoscopic particles—for example, fluorescent (CdS, CdSe),[1,2] metallic (Au, Ag, Cu),[3−5] or polymeric (polystyrene)[6]—have recently attracted considerable scientific attention due to their potential applications in corrosion protection,[7] crack-resistant electrodes,[8] heterogeneous catalysis,[9] antireflective films,[10] displays,[11] and substrates for cell adhesion.[12] Although nanoparticles (NPs) can be tethered onto surfaces by a variety of chemical ligation schemes,[13−15] through NP electrodeposition,[16,17] Langmuir−Blodgett,[18] or sol−gel[19] techniques, these methods generally require substrate-specific procedures. In addition, preparation of multicomponent, multilayer nanoparticle coatings on different types of materials remains challenging and has so far been limited to layer-by-layer schemes, in which layers of oppositely charged NPs are sequentially deposited onto the substrate.[20] Here, we describe a conceptually different and versatile approach to multicomponent coatings, in which metal core nanoparticles of different types and opposite charges are interspersed within each deposited NP monolayer. In our method, the coatings are plated from aqueous suspensions containing charged nanoparticles. Remarkably, while neither positively nor negatively charged particles alone absorb onto the substrates, their mixtures adsorb cooperatively and deposit layers stabilized by favorable electrostatic interactions between oppositely charged NPs and by residual hydrogen-bonding and van der Waals interactions between the particles and the substrate. Cooperative adsorption occurs readily onto a variety of materials (glasses, polymers, elastomers, and semiconductors) and gives coatings whose elemental composition (here, Au, Ag, Pd, and their combinations) and density can be regulated by the composition and the pH of the plating solution. The coatings are stable in common organic solvents and can be used in applications ranging from antibacterial protection to plasmonics. The practically appealing features of this system are its simplicity and generality, ability to coat large areas and nonplanar surfaces (including micropatterned ones), flexibility in tailoring surface composition, high degree of control over the coatings' thickness, and the reusability of the plating solutions.

(1) Coe-Sullivan, S.; Steckel, J. S.; Woo, W. K.; Bawendi, M. G.; Bulovic, V. *Adv. Funct. Mater.* **2005**, *15*, 1117−1124.
(2) Dabbousi, B. O.; Murray, C. B.; Rubner, M. F.; Bawendi, M. G. *Chem. Mater.* **1994**, *6*, 216−219.
(3) Kiely, C. J.; Fink, J.; Brust, M.; Bethell, D.; Schiffrin, D. J. *Nature* **1998**, *396*, 444−446.
(4) Kiely, C. J.; Fink, J.; Zheng, J. G.; Brust, M.; Bethell, D.; Schiffrin, D. J. *Adv. Mater.* **2000**, *12*, 640−643.
(5) Dong, T. Y.; Wu, H. H.; Lin, M. C. *Langmuir* **2006**, *22*, 6754−6756.
(6) Ahn, J. S.; Hammond, P. T.; Rubner, M. F.; Lee, I. *Colloids Surf. A−Physicochem. Eng. Asp.* **2005**, *259*, 45−53.
(7) Shen, G. X.; Chen, Y. C.; Lin, C. J. *Thin Solid Films* **2005**, *489*, 130−136.
(8) Kim, T. J.; Son, D.; Cho, J.; Park, B.; Yang, H. *Electrochim. Acta* **2004**, *49*, 4405−4410.
(9) Lee, S. W.; Drwiega, J.; Wu, C. Y.; Mazyck, D.; Sigmund, W. M. *Chem. Mater.* **2004**, *16*, 1160−1164.
(10) Prevo, B. G.; Hwang, Y.; Velev, O. D. *Chem. Mater.* **2005**, *17*, 3642−3651.
(11) Currie, E. P. K.; Tilley, M. *J. Soc. Inf. Displays* **2005**, *13*, 773−780.
(12) Kommireddy, D. S.; Sriram, S. M.; Lvov, Y. M.; Mills, D. K. *Biomaterials* **2006**, *27*, 4296−4303.
(13) Musick, M. D.; Keating, C. D.; Lyon, L. A.; Botsko, S. L.; Pena, D. J.; Holliway, W. D.; McEvoy, T. M.; Richardson, J. N.; Natan, M. J. *Chem. Mater.* **2000**, *12*, 2869−2881.
(14) Chen, S. W. *Langmuir* **2001**, *17*, 2878−2884.
(15) Niemeyer, C. M.; Ceyhan, B.; Noyong, M.; Simon, U. *Biochem. Biophys. Res. Commun.* **2003**, *311*, 995−999.
(16) Zhao, L. Y.; Eldridge, K. R.; Sukhija, K.; Jalili, H.; Heinig, N. F.; Leung, K. T. *Appl. Phys. Lett.* **2006**, *88*.
(17) Quinn, B. M.; Dekker, C.; Lemay, S. G. *J. Am. Chem. Soc.* **2005**, *127*, 6146−6147.
(18) Paul, S.; Pearson, C.; Molloy, A.; Cousins, M. A.; Green, M.; Kolliopoulou, S.; Dimitrakis, P.; Normand, P.; Tsoukalas, D.; Petty, M. C. *Nano Lett.* **2003**, *3*, 533−536.
(19) Fan, H. Y.; Wright, A.; Gabaldon, J.; Rodriguez, A.; Brinker, C. J.; Jiang, Y. B. *Adv. Funct. Mater.* **2006**, *16*, 891−895.
(20) Lee, D.; Rubner, M. F.; Cohen, R. E. *Nano Lett.* **2006**, *6*, 2305−2312.

Experimental Section

Our experiments were based on gold (5.8 nm metal core diameter; dispersity $\sigma = 11\%$), silver (5.3, 5.4, and 6.6 nm; $\sigma = 15$, 40, and 17%, respectively), and palladium (5.3 nm; $\sigma = 12.7\%$) nanoparticles prepared as described previously.[21,22] Positive charges were introduced onto the NPs[23] by covering them with a self-assembled monolayer (SAM)[24] of *N*,*N*,*N*-trimethyl(11-mercaptoundecyl)ammonium chloride (TMA, ProChimia Poland); negatively charged NPs were coated with mercaptoundecanoic acid (MUA, ProChimia; Figure 1a). The coating NP solutions were prepared by deprotonating MUA NPs at pH = 11[25] and titrating a solution of NPs of either polarity with small aliquots of a solution containing oppositely charged particles (Figure 1a). As we have shown before,[22,23,26] the titrated solutions remained stable until precipitating rapidly at the point when the charges of the nanoparticles were neutralized (i.e., when $\sum Q_{NP(+)} + \sum Q_{NP(-)} = 0$). The electroneutral nanoparticle precipitate thus obtained (from 0.5−2 mM solutions in terms of atoms of each metal) was washed several times with water to remove salts, redissolved in deionized (DI) water at 60−65 °C, and finally microfiltered to give a stable (for weeks) 0.5−4 mM solution[23,26] containing oppositely charged NPs in equal proportions. Immediately prior to use, the pH of the solution was adjusted to a desired value (optimally, pH ≈ 7; see discussion below) by dropwise addition of HCl or NMe_4OH.

The coatings were prepared as follows (Figure 1b,c). First, a desired substrate [e.g., borosilicate glass, poly(dimethylsiloxane) (PDMS), polystyrene, polyethylene, poly(methyl methacrylate) (PMMA), silicon, GaAs, or ITO] was washed with water followed by acetone and then oxidized in a plasma cleaner (Plasma Prep II, SPI) with air plasma for 15−120 min. The substrate was then immersed in the NP solution for ~6 h, after which it was washed with DI water (pH ≈ 5.5) and dried under a nitrogen stream. For all materials investigated, this procedure resulted in a uniform NP coating, which for metal NPs exhibiting surface plasmon resonance (Au, Ag) gave rise to a characteristic hue on transparent substrates (e.g., pink/purple for coatings containing AuNPs; Figure 1c). Closer inspection under scanning electron microscopy (SEM) revealed that the coatings had the nanoparticles arranged in a monolayer characterized by ~65% surface coverage for all hydrophilic substrates (Figures 1c, 2a). Interestingly, the adsorption process was self-terminating in the sense that the amount of adsorbed NPs did not increase after about the first 6 h of soaking. On the other hand, additional NPs could be deposited by washing the existing coating with water, drying for ~20 s under a stream of dry air or nitrogen, and then re-immersing in the plating solution. Each washing−drying−soaking cycle caused the coating's optical absorption to increase by a constant amount corresponding to additional ~25% of the initially deposited NPs (Figure 1d).

Results and Discussion

1. Factors Influencing Coating Formation. The quality and composition of the coatings were influenced by several factors. Specifically, we observed the following: (1.1) No coatings form on substrates that have not been oxidized prior to soaking in the NP solution. (1.2) No adsorption onto any of the oxidized substrates occurs from solutions containing only negatively charged MUA particles (Figure 2d); residual absorption (~3−5% surface coverage, Figure 2c) is observed with NPs coated with positively charged TMA particles.[27] Dense coatings form only from solutions containing NPs of *both* polarities (Figures 1c, 2a). (1.3) Adsorption is maximized when the pH of the soaking solution is adjusted close to neutral (Figure 2a vs Figure 2e,f). (1.4) Similarly, maximal adsorption is observed from electroneutral solutions (i.e., containing equal numbers of MUA

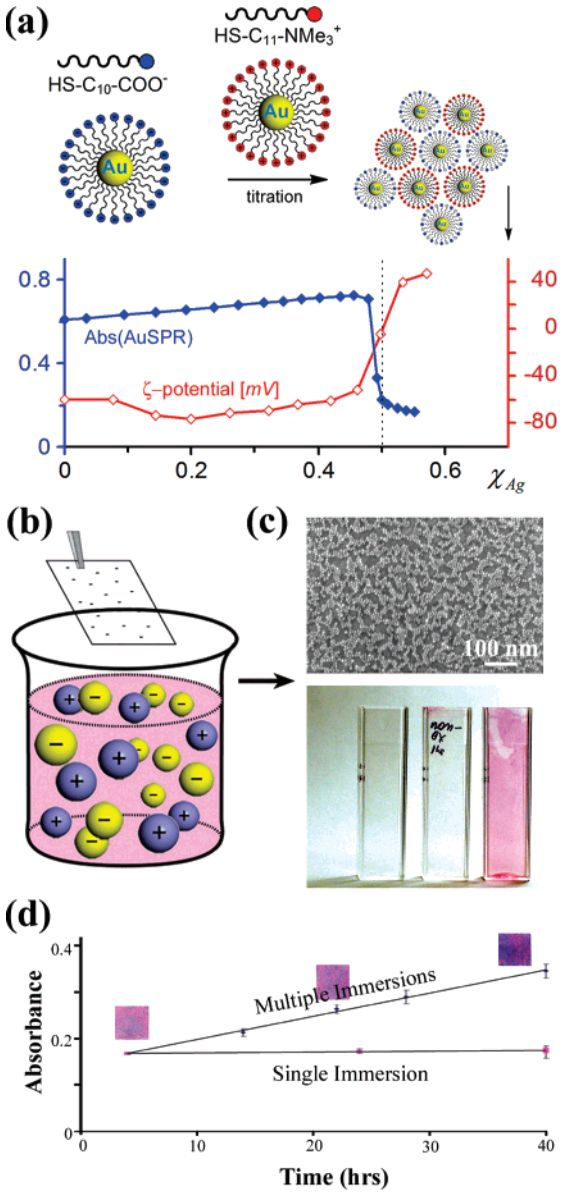

Figure 1. (a) Precipitation of oppositely charged nanoparticles monitored by UV−vis spectroscopy (blue curve) and ζ-potential measurements (red curve). Precipitation is sharp and occurs when the charges on the NPs of opposite polarities are compensated (here, at a 1:1 ratio of 5.8 nm AuTMA and 5.8 nm AuMUA nanoparticles) and the overall surface potential goes to zero. (b) Schematic illustration of the coating procedure. (c) An SEM image of Au/Ag coating formed on Si and the optical pictures of PMMA cuvettes not exposed to the Au/Ag NP plating solution (left), immersed in this solution for 1 h but not oxidized prior to immersion (middle), and plasma-oxidized and then immersed for 1 h (right). (d) Absorption of AgTMA−AuMUA coatings ($\lambda_{max} = 557-561$ nm) for a single and multiple immersions in the plating solution. With single immersion, the absorbance stabilizes after ca. 6 h. When, however, the coatings are sequentially deposited, washed, and dried, their optical density increases linearly with the number of deposition cycles (indicated by markers on the upper line). The images show glass slides coated once, three times, and five times.

(21) Kalsin, A. M.; Grzybowski, B. A. *Nano Lett.* **2007**, *7*, 1018−1021.
(22) Kalsin, A. M.; Kowalczyk, B.; Wesson, P.; Paszewski, M.; Grzybowski, B. A. *J. Am. Chem. Soc.* **2007**, *129*, 6664−6665.
(23) Kalsin, A. M.; Fialkowski, M.; Paszewski, M.; Smoukov, S. K.; Bishop, K. J. M.; Grzybowski, B. A. *Science* **2006**, *312*, 420−424.
(24) Witt, D.; Klajn, R.; Barski, P.; Grzybowski, B. A. *Curr. Org. Chem.* **2004**, *8*, 1763−1797.
(25) Leopold, M. C.; Black, J. A.; Bowden, E. F. *Langmuir* **2002**, *18*, 978−980.
(26) Kalsin, A. M.; Pinchuk, A. O.; Smoukov, S. K.; Paszewski, M.; Schatz, G. C.; Grzybowski, B. A. *Nano Lett.* **2006**, *6*, 1896−1903.

(27) These effects did not depend on the nature of the metal core, but only on the properties of the SAM coating the NPs.

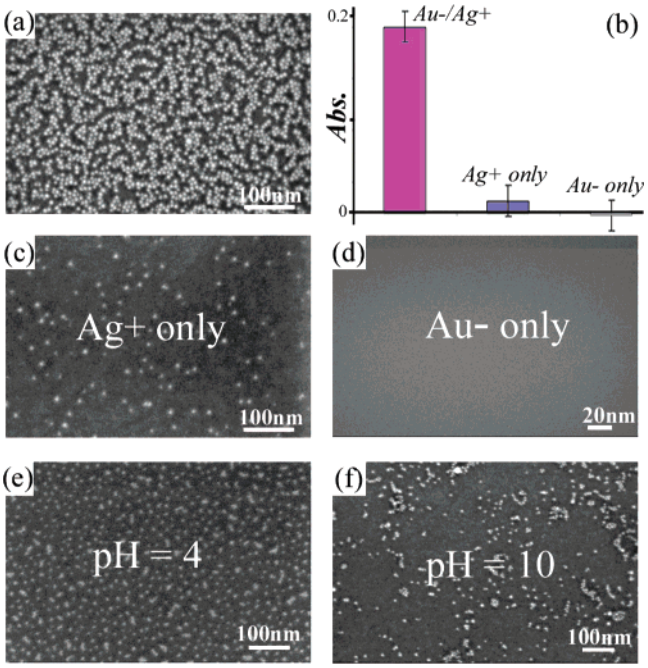

Figure 2. (a) SEM image of a typical Au/Ag coating deposited on oxidized Si from a pH = 7 solution containing oppositely charged NPs (here, AgTMA and AuMUA). The pink bar in (b) gives the coating's absorbance, $A \approx 0.18 \pm 0.015$, at $\lambda_{max} = 557-561$ nm. The blue bar ($A \approx 0.012 \pm 0.015$) corresponds to a much less dense coating deposited from a solution containing only positively charged silver nanoparticles. An image of this coating is shown in (c). When the solution contains only negatively charged NPs, no deposition is observed ($A \approx -0.002 \pm 0.015$), as illustrated by an SEM image in (d). With either (e) acidic or (f) basic pH's of the plating solutions, the forming coatings are less dense than at pH = 7.

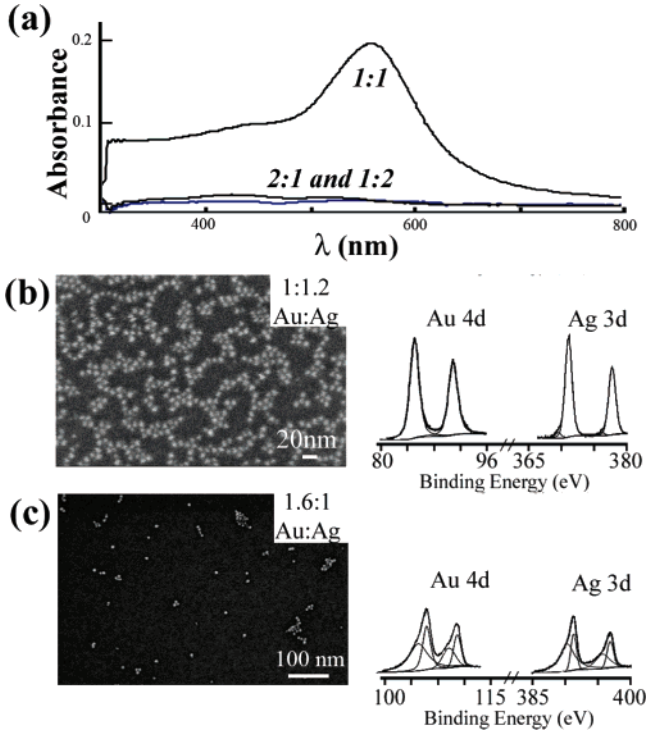

Figure 3. (a) UV−vis spectra of glass slides coated from solutions containing different proportions of AuMUA and AgTMA nanoparticles, 1:1, 2:1, and 1:2. The 1:1 ratio yields a much denser coating than either 2:1 or 1:2. (b) AuMUA/AgTMA coating prepared from solution containing 20% excess of AgTMAs. The XPS spectrum on the right shows that, despite unequal NP concentrations in solution, the coating has approximately equal numbers of Au and Ag NPs. (c) Analogous experiment with 60% excess AuMUAs in solution. The coating is very sparse but is composed of equal proportions of Au and Ag NPs.

and TMA-coated NPs), and addition of excess NPs of either type lowers the degree of surface coverage (Figure 3). (1.5) At the same time, XPS measurements show that, irrespective of solution concentrations, the relative surface concentrations of the adsorbed MUA and TMA NPs are always roughly equal (Figure 3b,c). (1.6) Finally, we note that, for the deposition of multilayers, drying of an already existing coating is crucial. Control experiments show that coatings washed and re-immersed into the plating solution without drying do not absorb any additional NPs, even with prolonged (days) soaking times.

2. Theoretical Model and Mechanism of Coating Formation. To rationalize these observations, we modeled the experimental system as a two-dimensional surface of constant area, A, in equilibrium with a NP solution of fixed chemical potential, μ, and temperature, T (Figure 4a). Using the Grand Canonical Monte Carlo (GCMC) scheme with periodic boundary conditions, we then investigated the influence of electrostatic, van der Waals, and hydrogen-bonding interactions (Figure 4b) on the coating's density and equilibrium composition.

2.1. Electrostatic Interactions. Electrostatic interactions between charged NPs in ionic solution and between the NPs and the substrates were derived from the appropriate electrostatic potentials, φ, via thermodynamic integration[28,29] and accounted for "charge regulation" at the NPs' surface—that is, for the equilibrium between counterions adsorbed onto the charged surfaces and those "free" in solution. Briefly, the electrostatic potential around the NPs or the substrate is well approximated by the linearized Poisson−Boltzmann (PB) equation,[30] $\nabla^2\varphi = \kappa^2\varphi$, where $\kappa^{-1} = (\epsilon_0\epsilon k_B T/2ce^2)^{1/2}$ is the Debye screening length (~10 nm for our system), c is the monovalent salt concentration, e is the fundamental charge, ϵ_0 is the permittivity of a vacuum, ϵ is the dielectric constant of the solvent, k_B is Boltzmann's constant, and T is the temperature. The adsorption equilibrium at a positively charged surface (here, TMA-coated NPs), presenting N_T positively charged groups, A^+, in a solution containing negatively charged counterions, B^-, is determined by $N_{A^+}C_{B^-}/N_{AB} = K_+ \exp(e\varphi_s/k_BT)$,[31] where N_{A^+} and N_{AB} are, respectively, the numbers of counterion-free and counterion-bound surface ligands ($N_{A^+} + N_{AB} = N_T$), C_{B^-} is the concentration of counterions in solution, K_+ is the equilibrium constant in the absence of any external fields, and φ_s is the electrostatic potential at the surface.[32] From this relation, the surface charge

(28) Carnie, S. L.; Chan, D. Y. C.; Gunning, J. S. *Langmuir* **1994**, *10*, 2993−3009.
(29) Verwey, E. J. W.; Overbeek, J. T. G. *Theory of the Stability of Lyophobic Colloids*; Elsevier: New York, 1948.
(30) This approximation is reasonable for surface potentials less than ~60 mV such as those studied here. See ref 32.
(31) Carnie, S. L.; Chan, D. Y. C. *J. Colloid Interface Sci.* **1993**, *161*, 260−264.
(32) Measurements performed on a Brookhaven Instruments Zeta-PALS analyzer for solutions (~1 mM ionic strength and pH ≈ 10) gave the magnitudes of surface potential 30−60 mV for different types of NPs used (φ_s was negative for MUA NPs and positive for TMA ones; for details see refs 21 and 22). For the substrates we used, the values of surface potentials reported in the literature are around −0.05 V. For instance, for plasma-oxidized glasses and siloxanes presenting SiOH groups, $\varphi_{surf} \approx -0.03$ to −0.09 V.[33−35] For polymers, oxidation introduces surface groups such as carboxylic acids and phenols[36] and gives rise to surface ζ-potentials that are ~ −0.09 V for polycarbonate, ~ −0.05 V for polystyrene and polyethylene, and ~ −0.03 V for PMMA.[37] For ITO, the ζ-potential has been measured[38] to be ~ −0.04 V.
(33) Gu, Y. G.; Li, D. Q. *J. Colloid Interface Sci.* **2000**, *226*, 328−339.
(34) Kirby, B. J.; Hasselbrink, E. F. *Electrophoresis* **2004**, *25*, 187−202.

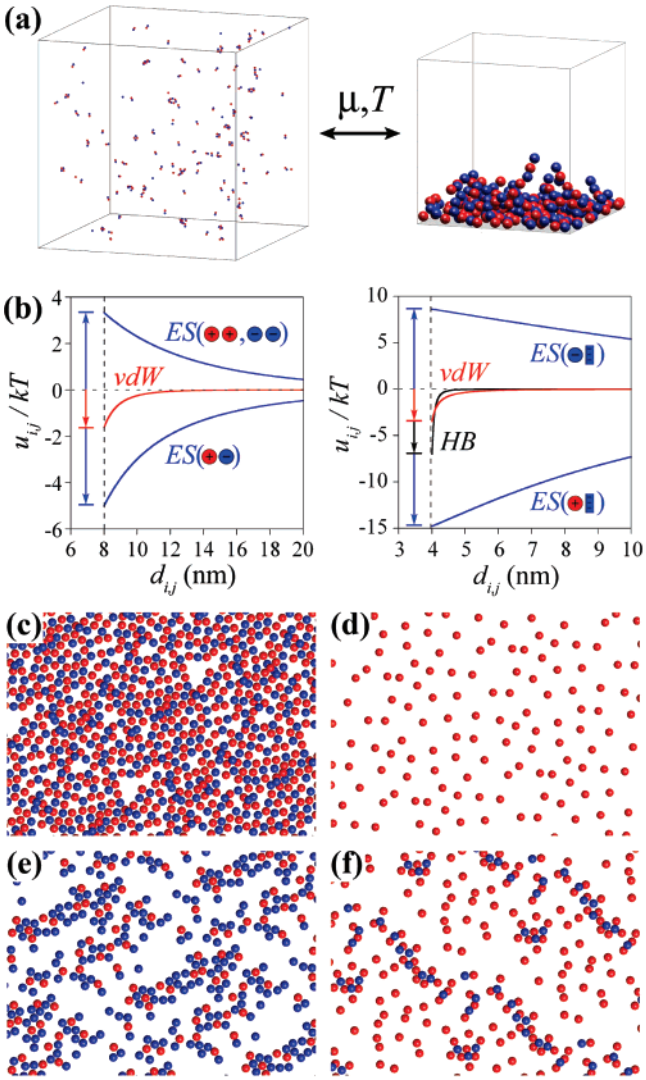

Figure 4. (a) Periodic simulation cell ("reservoir") of dimensions 1 μm × 1 μm × 1 μm in equilibrium (i.e., at constant chemical potential, μ, and temperature, T) with a smaller cell (typically, 150 nm × 150 nm × 150 nm) with the substrate at the $z = 0$ plane. Red spheres denote positively charged TMA NPs; blue spheres are negatively charged MUA NPs. (b) Calculated electrostatic (ES), van der Waals (vdW), and hydrogen bond (HB) potentials at pH = 7 for two spheres (left) and for a sphere and surface (right) as a function of their separation. The arrows give the magnitudes of the various types of interactions at contact. (c) Dense coating obtained from an equimolar mixture of positive and negative NPs at pH = 7. (d) Sparse coatings from a solution of positively charged NPs at pH = 7 (note: negative NPs give no coating on a negatively charged surface). (e) At low pH = 4, hydrogen bonding increases, but the net charges of the negatively charged surfaces (i.e., MUA covered NPs and the substrate) decrease. As a result, the coatings become sparser than at pH = 7. (f) Likewise, high pH = 10 decreases the magnitude of hydrogen-bonding interactions and also leads to low surface coverages.

density, σ, may be expressed as $\sigma = e\rho/[1 + (C_{B^-}/K_+)\exp(e\varphi_s/k_BT)]$, where $\rho = N_T/4\pi R^2$ is the surface density of charged groups (e.g., $\rho \approx 2.6$ nm^{-2} for a TMA SAM[39] on a nanoparticle of metal core radius $R_c = 3$ nm). Assuming the dielectric constant of the TMA SAM ($\epsilon_p \approx 2$) is small compared to that of the solvent ($\epsilon \approx 80$ for water), the surface charge is related to the potential at the NP surface by $\sigma = -\epsilon_0\epsilon\nabla\varphi\bar{n}$, where $\bar{n}$ is the outward surface normal. Equating the two relations for σ provides the necessary boundary condition for a positively charged NP. For the case of negatively charged MUA NPs or for the oxidized substrates, the reasoning is similar, but it is necessary to account for two equilibrium relations, one due to the physical adsorption of counterions and the second due to the protonation/deprotonation of surface groups (e.g., COOH for MUA NPs, Si−OH for oxidized glass or PDMS substrates). Accounting for these equilibria, the charge density of these negatively charged surfaces is given by $\sigma = -e\rho/[1 + (C_{H^+}/K_A + C_{B^+}/K_-)\exp(-e\varphi_s/k_BT)]$, where C_{H^+} is the concentration of H^+ ions in solution, K_A is the acid/base dissociation constant of the ionizable groups ($pK_a \approx 5$ for MUA NPs,[25,40] $pK_a \approx 7.5$ for glass[41]), C_{B^+} is the concentration of positively charged counterions in solution, and K_- is the equilibrium constant for counterion adsorption.

With the experimentally determined values of surface potentials[32] and with other parameters estimated above, the equilibrium constants are estimated as $K_- = K_+ \approx 0.06$ mM, and solving the PB equation for the case of two interacting NPs[28] and for the case of an NP interacting with a planar substrate yields the interaction potentials shown in Figure 4b.[42]

2.2. Van der Waals (vdW) Interactions. In addition to electrostatic forces, the NPs and the surface interact by attractive vdW interactions, which may be approximated using the Hamaker "hybrid" approximation,[44] in which the form of the vdW potential is taken from Hamaker pairwise summation, with Hamaker constants calculated from the more rigorous Lifshitz theory or taken from experiment. Specifically, for the NP−NP interactions,

$$u_{i,j}^{vdW} = \frac{A}{3}\left[\frac{R_c^2}{(d_{i,j}^2 - 4R_c^2)} + \frac{R_c^2}{d_{i,j}^2} + \frac{1}{2}\ln\left(1 - \frac{4R_c^2}{d_{i,j}^2}\right)\right]$$

where $R_c = 3$ nm is the radius of the metal core, d_{ij} is the distance between centers of spheres i and j, and the Hamaker constant $A \approx 4.0 \times 10^{-19}$ J for gold across water.[45] For the NP−surface interactions,

$$u_{i,surf}^{vdW} = \frac{A_{surf}}{6}\left[\frac{R}{(z_i - R)} + \frac{R}{(z_i + R)} + \ln\left(\frac{z_i - R}{z_i + R}\right)\right]$$

where $R = 4$ nm is the radius of a SAM-covered NP, z is the distance between the NP center and the plane of the surface,

(35) Lee, G. B.; Lin, C. H.; Lee, K. H.; Lin, Y. F. *Electrophoresis* **2005**, *26*, 4616−4624.
(36) Wiles, J. A.; Fialkowski, M.; Radowski, M. R.; Whitesides, G. M.; Grzybowski, B. A. *J. Phys. Chem. B* **2004**, *108*, 20296−20302.
(37) Kirby, B. J.; Hasselbrink, E. F. *Electrophoresis* **2004**, *25*, 203−213.
(38) Tseng, W. J.; Tzeng, F. *Colloids Surf. A−Physicochem. Eng. Asp.* **2006**, *276*, 34−39.
(39) Sellers, H.; Ulman, A.; Shnidman, Y.; Eilers, J. E. *J. Am. Chem. Soc.* **1993**, *115*, 9389−9401.
(40) Lide, D. R. *CRC Handbook of Chemistry and Physics on CD-ROM*, 87th ed.; CRC Press: Boca Raton, FL, 2007.
(41) Hiemstra, T.; Dewit, J. C. M.; Vanriemsdijk, W. H. *J. Colloid Interface Sci.* **1989**, *133*, 105−117.
(42) The interesting feature of these dependencies is that the attractive energy between oppositely charged NPs at contact is greater in magnitude than the repulsive energy of like-charged NPs at the same distance. This effect is due to the desorption of counterions from between oppositely charged NPs (where electrostatic potential is low) and adsorption of counterions into the region between like-charged NPs (where potential is high). For further details, see ref 43.
(43) Bishop, K. J. M.; Grzybowski, B. A. *Chem. Phys. Chem.* **2007**, *8*, 2171−2176.
(44) Parsegian, V. A. *Van der Waals forces: a handbook for biologists, chemists, engineers, and physicists*; Cambridge University Press: New York, 2006.
(45) Israelachvili, *Intermolecular and Surface Forces*, 2nd ed.; Academic Press: New York, 1991.

and the Hamaker constant for the NP−surface interaction, $A_{surf} \approx 5.3 \times 10^{-21}$ J, is similar for all the surfaces studied here.[46]

2.3. Hydrogen Bonding. Finally, to account for the pH dependence of coating density (cf. Figure 2), we consider hydrogen bonding between the MUA particles (TMA NPs are neither H-bond donors nor acceptors) and between these particles and the polar groups (OH, COOH, phenols, and their deprotonated forms[47]) on the surface. These favorable interactions can be related to the number of hydrogen bonds at contact, estimated as $N_{HB} \approx A_{eff}\rho(\theta_{1A}\theta_{2D} + \theta_{1D}\theta_{2A})$, where ρ is the density of H-bonding groups on the surface, θ_{iA} and θ_{iD} are the fractions of such groups on surface i that are, respectively, H-bond accepting and H-bond donating, and A_{eff} is the effective area of contact between the surfaces ($A_{eff} \approx 2\pi R\delta$ for two like-sized spheres and $A_{eff} = 4\pi R\delta$ for a sphere in contact with a planar surface,[45] where $\delta = 0.2$ nm is a characteristic H-bond length). At neutral pH, only the substrate is partially protonated (e.g., ∼16% for glass at pH = 7), resulting in $N_{HB} \approx 4.2$ possible bonds between each MUA NP and the substrate. With these approximations and using the typical energy of a hydrogen bond ∼10 kJ/mol,[45] the energies of NP/NP and NP/surface hydrogen bonding in aqueous solution at pH = 7 can be conservatively estimated at, respectively, $U \approx 0$ and $U_{surf} \approx -7kT$ (these increase to $U \approx 1kT$ and $U_{surf} \approx -15kT$ at pH = 4). While these values give only the magnitudes of H-bonding interactions at contact, we also account for their distance dependence using the so-called Boltzmann-averaged "Keesom" potentials,[45,48] which after integration over the interacting domains (sphere−sphere or sphere−plane) give

$$u_{i,j}^{HB} = \frac{2U\delta^3 R}{d_{i,j}}\left[\frac{1}{(d_{i,j}+2R)^3} - \frac{2}{d_{i,j}^3} + \frac{1}{(d_{i,j}-2R)^3}\right] \quad \text{and}$$

$$u_{i,surf}^{HB} = U_{surf}\,\delta^3\left[\frac{1}{(z_i-R)^3} - \frac{1}{(z_i-R)^3}\right] \qquad (2)$$

where $d_{i,j} = 2R + \delta$ is the distance of closest approach.

2.4. Simulations. With all the these individual contributions, the overall energy of the system can be written as

$$U_{tot} = \sum_{i=1}^{N}\sum_{j\geq i}^{N}(u_{i,j}^{ES} + u_{i,j}^{vdW} + u_{i^*,j^*}^{HB}) + \sum_{i=1}^{N}(u_{i,surf}^{ES} + u_{i,surf}^{vdW} + u_{i^*,surf}^{HB}) \qquad (3)$$

where N is the total number of NPs in the periodic-boundary simulation cell (typically, 300; see Figure 4a), and the star (*) denotes that hydrogen-bonding interactions are only included for negatively charged (MUA-coated) NPs. The phase space of the adsorbing particles can then be sampled using the traditional GCMC algorithm,[49−51] in which MC moves consist of particle insertion, displacement, or removal attempts accepted according to the Boltzmann criterion. The results of the simulations (whose technical details will be published separately) agree with experimental observations (cf. points 1.1−1.6) and lead to the following conclusions:

(i) The residual charge on the surface is necessary for the NP adsorption to occur.

(ii) The fact that no or only very sparse coatings form from solutions of like-charged particles is a consequence of electrostatic repulsions between the adsorbed NPs (for TMA NPs) and/or the NPs and the charged surface (for MUA NPs) (Figure 4c,d). Interestingly, this conclusion is also supported by a qualitative, thermodynamic argument in which the number of the NPs adsorbed per unit area, n, is estimated by equating the chemical potentials, μ, of the NPs in the solution phase and in a thin (on the order of particle radius, R) layer near the surface: $\mu_{sol}^0 + kT \ln \rho_{sol} = \mu_{surf}^0 + kT \ln (n/R)$, where $\rho_{sol} \approx 0.3$ μM is the number density of NPs in solution (∼1.8×10^{14} NPs/mL). Rearranging this expression gives $n = R\rho_{sol}\exp(-E_{ad}/kT)$, where E_{ad} is the energy of NP adsorption. For example, for a TMA NP coating at equilibrium, the favorable energy between a NP and the oppositely charged substrate is $\sim -15kT$ at contact, which is partly offset by a repulsive NP−NP energy of $\sim 7kT$ to give $E_{ad} \approx -8kT$. With these estimates, the expected coating density is only $n = 0.002$ nm^{-2} (i.e., ∼10% surface coverage for $R = 4$ nm particles), close to the sparse TMA coatings observed in experiment and in numerical simulations (see Figure 4d). Of course, for MUA NPs, the adsorption energy is strongly unfavorable, and n is negligible.

(iii) Electrostatic interactions alone are unable to induce dense coatings, even from mixtures of oppositely charged NPs. This is so because the net adsorption energy of oppositely charged NPs is still not sufficiently favorable to form dense coatings ($n \approx 0.02$ nm^{-2}) in equilibrium with a dilute solution phase [which is also entropically favored; cf. the $kT \ln \rho$ term in point (ii) above]. Thus, coating formation requires the help of attractive vdW and HB interactions (cf. Figure 4b, right).

(iv) Overall, adsorption is a cooperative process requiring participation of NPs of both polarities and is facilitated by vdW and H-bonding interactions.

(v) Maximal degree of adsorption observed at pH = 7 reflects the optimal balance between hydrogen-bonding and electrostatic interactions. At lower pH's, both the substrate and the MUA groups on the NPs are partly protonated—this allows for the formation of more hydrogen bonds but decreases surface charges and favorable electrostatic interactions between MUA and TMA NPs and between the substrate and TMA NPs. Consequently, the coatings that form are sparse. Conversely, at high pH, when both MUAs and the ionizable groups on the substrate are deprotonated, H-bond interactions are negligible, also resulting in less dense coatings. These effects are reproduced in the simulations for pH = 4 (Figure 4e) and pH = 10 (Figure 4f).

(vi) Since the magnitudes of the van der Waals forces are similar for NPs made of different metals (both because the NP−substrate interaction is dominated by the SAM and because the

(46) NP−surface Hamaker constants were estimated using an integral approximation of the Lifshitz theory combined with approximate forms for the dielectric permittivity (this approximation is described in detail in ref 45). In contrast to the NP−NP interactions, the NP−surface interaction is dominated by the SAM coating, which was allowed to approach the substrate down to a minimum distance of $\delta = 0.2$ nm. This value corresponds to a characteristic molecular length scale that has previously been shown to provide good estimates of vdW energies at contact[45] and is approximately equal to the distance of closest approach for hydrogen bonds (cf. discussion of H-bonding in the text).

(47) Joesten, M. D.; Schaad, L. J. *Hydrogen Bonding*; Marcel Dekker, Inc.: New York, 1974.
(48) Klajn, R.; Bishop, K. J. M.; Grzybowski, B. A. *Proc. Natl. Acad. Sci. U.S.A.* **2007**, *104*, 10305−10309.
(49) Allen, M. P.; Tildesley, D. J. *Computer Simulations of Liquids*; Clarendon Press: Oxford, 1987.
(50) Frenkel, D.; Smit, B., *Understanding Molecular Simulation*, 2nd ed.; Academic Press: New York, 2002.
(51) Norman, G. E.; Filinov, V. S. *High Temp. (USSR)* **1969**, *7*, 216−222.

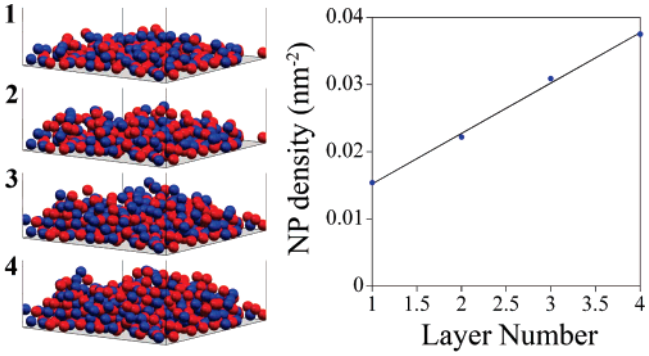

Figure 5. (Left) In layer 1, the bare substrate is first equilibrated with the NP plating solution, and all NPs within 1.25 particle diameters from the surface are then fixed in place, approximating the experimental process of drying (we note that allowing for limited "lateral" mobility of the NPs *in* the plane of the monolayer leads to qualitatively similar results). Fixed NPs act as a new, modified substrate onto which the next layer absorbs. The procedure is repeated sequentially to yield coatings of increasing thickness. (Right) The graph shows that the number of NPs deposited per unit area increases linearly (cf. Figure 1d) with the number of deposition cycles.

Hamaker constants for different metals are similar), adsorption is expected to depend predominantly on the charges and concentrations of the NP and on the properties of the coating ligands and not on the materials properties of the NPs' cores.

(vii) Finally, the necessity to dry existing coatings before additional NPs can be deposited can be rationalized by the removal of water and concomitant formation of H-bonds and specific electrostatic interactions (i.e., direct ion−ion pairs) that had previously been "screened" by hydration. As a result of these enhanced interactions, the NPs become irreversibly bound to the substrate (although they can have a limited degree of lateral mobility on the substrate, cf. Figure 5). When returned to the NP plating solution, the permanently coated surface provides a stable substrate for further absorption of oppositely charged NPs. This scenario was verified in simulations, in which the initial coating was "fixed" to the substrate and was then equilibrated with the NP solution. These simulations show (Figure 5) that the number of NPs per unit area increases linearly with each successive coating, as observed in experiment (cf. Figure 1d). The simulations also confirm that, when the coatings are not fixed prior to equilibration with the plating solution, no additional deposition occurs.

3. Coatings' Composition, Stability, and Applications. The trends identified in points (i)−(vii) above allow for the optimization of coating conditions and for the use of NPs of different types (i.e., having different metal cores) in various proportions. In particular, since the deposited coating always contains equal numbers of positively and negatively charged NPs (see Figure 3), but the identity of the metal cores does not affect particle/surface interactions [point (vi) above], it is possible to prepare coatings of arbitrary content of different metals. This is illustrated in Figure 6, showing examples of coatings composed of the NPs having the same metal cores (1:1 ratio of AgTMAs and AgMUA; Figure 6a), two different cores (1:1 AuMUAs and AgTMAs; Figure 6b), and even three different cores (1:1:2 AuTMA, AgTMA and PdMUA; Figure 6c). The plating solution for tri-component coating is prepared by first mixing equal volumes of equimolar AuTMA and AgTMA solutions and then titrating with a solution of Pd-MUAs until electroneutrality. The redissolved precipitate is then used for plating. This procedure can be extended to other compositions and metal combinations. For instance, a four-component (say, metals X,Y,Z,W) coating of elemental composition n_x:n_y:n_z:n_w could be prepared by first mixing like charged X-MUA and Y-MUA NPs in n_x:n_y proportion, titrating them with an n_z:n_w mixture of Z-TMA and W-TMA NPs until precipitation at the point of electroneutrality, and then plating the surface with the redissolved precipitate.

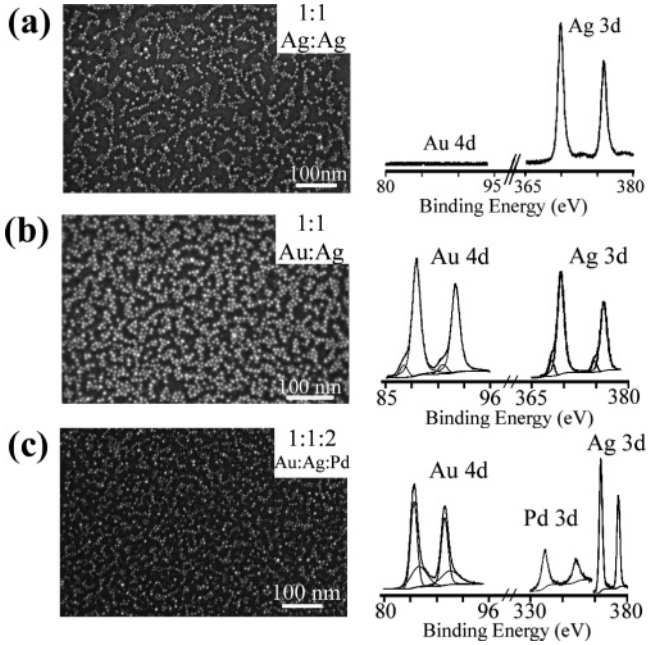

Figure 6. Coatings composed of NPs having the same or different metal cores. Left panels are SEM images; right panels give the corresponding XPS spectra and the composition of the coatings: (a) AgMUA/AgTMA; (b) AuMUA/AgTMA; (c) AuTMA/AgTMA/PdMUA.

The method is also suitable for coating nonplanar and microstructured surfaces. For example, Figure 7a shows a coating deposited on a surface of a cylindrical glass vial. In Figure 7b, an array of micrometer-wide lines, embossed on the surface of PDMS, is coated multiple times with NPs—as the SEM images indicate, the coating density is uniform both on the horizontal and on the vertical faces. Figure 7c has an image of a ZnO surface first microstructured using ASoMic[52−54] and then uniformly coated with Ag/Au NPs. From a practical perspective, it is worth mentioning that, since each coating cycle removes equal amounts of positively and negatively charged NPs, the composition of the plating solution remains unchanged, and this solution can be used in multiple deposition cycles onto the same or different substrates.

Despite the inherent water solubility of the constituent particles and the lack of their covalent attachment to the substrates, the deposited NP mono- and multilayers are stable against prolonged (weeks) soaking[55] in DI water and also in salt solutions (e.g., KCl) up to 1 M. The coatings are also stable in acetone, methanol, 0.2 M HCl, and dilute bases (e.g., 0.02 M NMe_4OH) for at least 48 h. On the other hand, they disintegrate rapidly when exposed to concentrated acids (e.g., >1 M HCl) or bases (e.g., 0.2 M NaOH or NMe_4OH).

(52) Smoukov, S. K.; Bishop, K. J. M.; Klajn, R.; Campbell, C. J.; Grzybowski, B. A. *Adv. Mater.* **2005**, *17*, 1361−1365.
(53) Campbell, C. J.; Smoukov, S. K.; Bishop, K. J. M.; Baker, E.; Grzybowski, B. A. *Adv. Mater.* **2006**, *18*, 2004−2008.
(54) Smoukov, S. K.; Grzybowski, B. A. *Chem. Mater.* **2006**, *18*, 4722−4723.
(55) The deposited films and the solutions in which they were soaked were periodically (every ∼24−48 h) monitored by UV−vis. No changes in either spectra were observed during soaking.

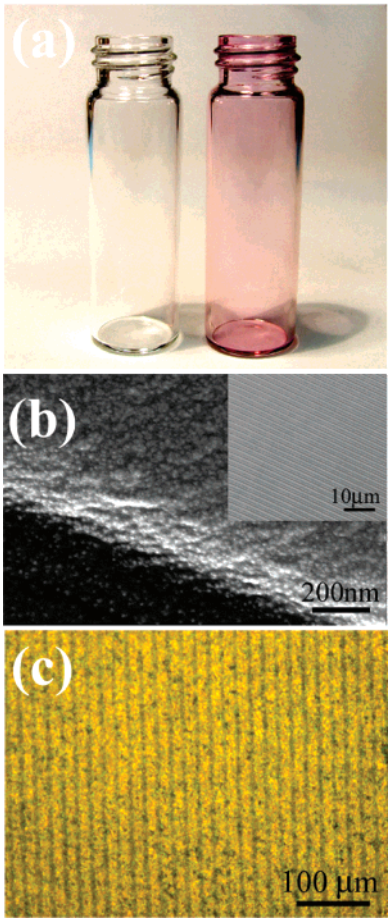

Figure 7. NP coatings on nonplanar and microstructured surfaces. Various curved and patterned surfaces coated with AuMUA/AgTMAs. (a) A coated glass vial (right) next to an uncoated one (left). (c) SEM image of a corner of a 1 μm line pattern (750 nm deep) in oxidized PDMS covered with NPs. The inset shows a large-area SEM image. (c) Optical micrograph of ZnO microstructured by ASoMic[52−54] with 10 μm lines and then coated with nanoparticles.

The stability of coatings in aqueous environments suggests their uses in biologically oriented applications. Figure 8 provides one such example, where AgTMA/AgMUA NP monolayers deposited on glass and PDMS disks exhibit excellent antibacterial properties (likely due to silver ion release)—evidenced by the pronounced zone of inhibition around the coated disks—against both Gram-positive (*Streptococcus aureus*) and Gram-negative (*Escherichia coli*) bacteria (other materials we coated include PS, polyester, and PET/PETG copolymer.) Although the inhibition of bacterial growth by colloidal silver is well known and widely used, the commonly used coatings contain significantly more silver[56,5] than our NP monolayers (~23 mg of Ag/m^2). The facts that our coatings retain antibacterial activity for months (so far), are not cytotoxic (Figure 8b), and have an easily discernible orange hue make them attractive as protective films for home-appliance products and medical devices (e.g., on catheters or siloxane implants, cf. Figure 8a).

Finally, coatings containing metal particles exhibiting surface plasmon resonance (SPR) are interesting in the context of plasmonic-based detection systems. This is illustrated in Figure

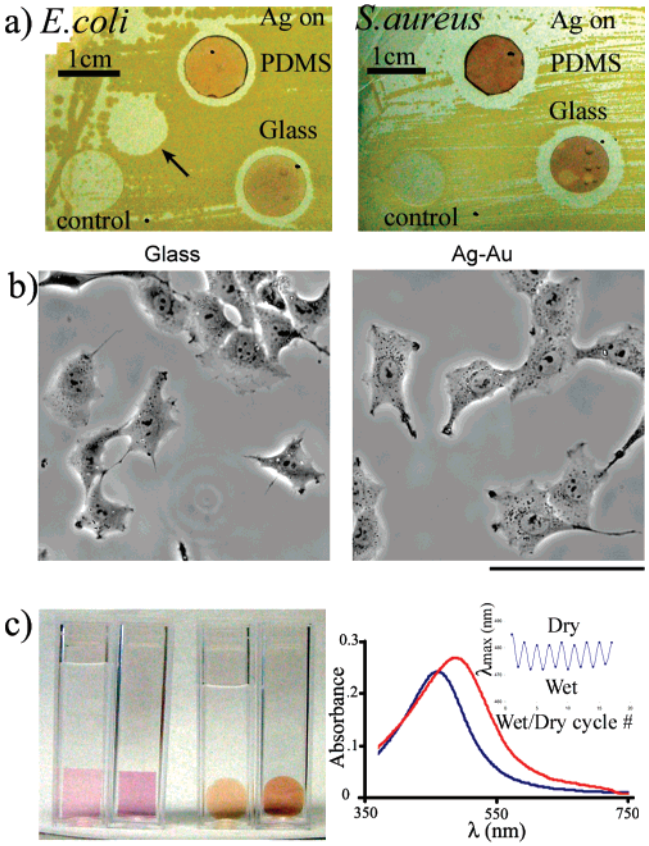

Figure 8. (a) Pronounced zones of inhibitions around glass and PDMS disks in bacterial cultures (at 15 h of growth) demonstrate antibacterial activity of Ag(+)/Ag(−) monolayers against both Gram-negative (*E. coli*, left) and Gram-positive (*S. aureus*, right) bacteria (likely due to silver ion release). Note the absence of inhibition around uncoated glass controls. The upper of the two blank circles (indicated by an arrow) in the left picture corresponds to the experiment in which an NP-coated PDMS disk was initially placed into the culture for 2−3 s and then removed. The lack of bacterial growth over this region demonstrates instantaneous, contact-killing properties of the coatings. (b) Rat-2 cells on glass coated with fibronectin and on glass coated with antibacterial AgNPs (no fibronectin) adhere, spread, and move with the same morphologies and motility characteristics. Unlike bacteria shown in (a), mammalian cells on NP coatings remain live and motile (in L15 medium supplemented with 10% serum) for at least several days. Scale bar = 50 μm. (c) Glass pieces coated with Ag(+)/Au(−) (purple) and Ag(+)/Ag(−) coatings (orange) show color differences when wet or dry (left and right vials in each pair, respectively). The spectra on the right show significant broadening of the absorption band upon drying, which is reversible upon subsequent wetting. The inset shows reversible shifts of the absorption maximum over 9 wetting/drying cycles.

8c, where the coatings reversibly change color upon immersion in water. Interestingly, the wavelength of maximum adsorption, λ_{max}, is shorter in water than in air, thus ruling out possible explanations based on the change of refractive index, n, around the NPs (where one would expect[58] λ_{max} to increase with n). Instead, broadening of the SPR band upon drying suggests that the NPs in dry coatings are aggregated but disperse upon hydration. This scenario would imply that while the NPs are bound to the surface, they retain a certain degree of lateral mobility within the monolayer (cf. Figure 4), which is plausible given that these particles are not covalently bound to the surface. More work is needed to understand this interesting phenomenon in quantitative detail.

(56) Song, J. S.; Lee, S.; Cha, G. C.; Jung, S. H.; Choi, S. Y.; Kim, K. H.; Mun, M. S. *J. Appl. Polym. Sci.* **2005**, *96*, 1095−1101.
(57) Zaporojtchenko, V.; Podschun, R.; Schurmann, U.; Kulkarni, A.; Faupel, F. *Nanotechnology* **2006**, *17*, 4904−4908.
(58) Tanahashi, I.; Yamazaki, F.; Hamada, K. *Chem. Lett.* **2006**, *35*, 454−455.

Conclusions

In summary, we described a novel class of electrostatically "patchy" nanoparticle coatings that form on different types of materials via a cooperative adsorption mechanism. The most appealing features of this electrostatics-based approach are its ability to coat large areas of arbitrary topographies and the high degree of control over the coatings' densities and compositions. The major difference between this method and the alternative layer-by-layer schemes is that our method produces coatings in which oppositely charged NPs adsorb simultaneously and are interspersed within each deposited layer; in addition, it does not require substrate-specific functionalization to initiate adsorption. Future research could extend the work reported here to coatings composed of nanoparticles of different types (e.g., catalytically active NPs) and sizes. In the latter context, it would be interesting to examine whether different magnitudes of vdW and electrostatic forces between differently sized NPs[59] would affect coating uniformity and would lead to phase-separated NP films (e.g., with large particles clumping together due to stronger vdW forces).

Acknowledgment. This work was supported by the National Science Foundation (Grant No. CHE-0503673). B.A.G. gratefully acknowledges further financial support from the Pew Scholars Program in Biomedical Sciences, the Sloan Foundation, and the Camille Dreyfus Teacher-Scholar Program. K.J.M.B. was supported by a NSF graduate fellowship. The authors thank Dr. Maciej Paszewski and Timothy P. Gray for their help with the synthesis of PdNPs and XPS spectra.

JA075456W

(59) Shevchenko, E. V.; Talapin, D. V.; Kotov, N. A.; O'Brien, S.; Murray, C. B. *Nature* **2006**, *439*, 55−59.